Aluminum and vacancies in α-iron: Dissolution, diffusion, and clustering

H. Amara,[1] C. C. Fu,[2] F. Soisson,[2] and P. Maugis[3]
[1]*Laboratoire d'Etude des Microstructures, ONERA-CNRS, BP 72, 92322 Châtillon Cedex, France*
[2]*Service de Recherches de Métallurgie Physique, DMN-SRMP, CEA Saclay, 91191 Gif-sur-Yvette, France*
[3]*IM2NP, Université Aix-Marseille, 13397 Marseille, France*
(Received 21 December 2009; revised manuscript received 23 March 2010; published 3 May 2010)

First-principle calculations have been performed to study the electronic structure and energetics of the dissolution of aluminum in α-iron and the interaction between Al atoms and vacancies (V). We find that the formation of small V_nAl_m complexes ($n,m=0-4$) is energetically favorable. Their stability is mainly driven by strong Al-V attractions whereas Al-Al interactions are repulsive. Using *ab initio* predictions, a rate theory based model that accounts for the evolution of aluminum and vacancies created upon rapid quenching has been developed to explore the influence of Al in the presence of the V_nAl_m complexes in α-iron. Finally, using the Le Claire's diffusion model, the diffusion properties of solute Al are investigated.

DOI: 10.1103/PhysRevB.81.174101 PACS number(s): 61.72.jd, 71.15.Mb, 71.15.Nc

I. INTRODUCTION

The development of low-density steel is a very promising alternative in order to meet the industrial demand for high-performance material. Fe-Al based alloys are known as useful materials owing to medium-temperatures corrosion resistance, mechanical strength, and relative low density.[1–3] However, a large number of properties, such as creep, sintering, oxidation, and diffusion, are highly sensitive to the type and concentration of defects as well as the deviation from the stoichiometry.[4–6] It is well known that upon rapid quenching from elevated temperatures, iron aluminides retain a high concentration of thermal vacancies (V), which frozen, increase their yield strength and hardness at room temperature.[7,8] The technical application of these alloys is then restricted presently by poor ductility at low temperatures and low fracture toughness.[4,9]

For that reason, an exact systematic analysis of the defect formation and their characterization at atomic scale are decisively important for understanding of these systems. Several theoretical works have already focused on studying the FeAl intermetallic compounds[10–15] and their defects.[16–23] Most of those studies are mainly devoted to ordered structures, such as B2 or $D0_3$. They have concentrated on determining the stability and the precise property of the defects (vacancies, interstitials, impurities, etc.) in FeAl intermetallic alloy.

However, there are few studies related to the role of structural defects on the electronic structures, magnetic properties, and atomic bonding in dilute Fe-Al alloys, which should also help to give a better understanding of their behavior and mechanical properties. In particular, as these materials are sensitive to quench-in vacancies,[24,25] the combination of small radius Al atoms with vacancies has not been fully addressed and is of a particular interest. Indeed, one can suggest the possibility that V_nAl_m clusters can be formed during the production process and then affect the properties of the material. The aim of the present work is to investigate the properties of vacancies and defects in the FeAl system with the intention of understanding the stability of V_nAl_m clusters in very dilute case. The approach proposed here is to combine *ab initio* calculations, simple thermodynamic and Le Claire's diffusion models to gain a survey of the thermodynamic and diffusion properties of such systems.

The paper is organized as follows: all binding and migration energies were obtained by means of density-functional theory (DFT) calculations, which are presented in Sec. II. In Sec. III, we discuss the energetic, electronic, and magnetic properties of FeAl alloy in a B2 structure and its defects. Section IV, presents the thermodynamic properties of V_nAl_m clusters. The electronic properties and binding energies of Al-Al and Al-V interactions are analyzed in details to understand the behavior of V_nAl_m clusters. Finally, the diffusion properties of solute Al in iron are investigated in Sec. V

II. METHODOLOGY

DFT calculations have been performed using the SIESTA code[26] within the generalized gradient approximation (GGA). The pseudopotential and the localized basis set for Fe atoms are the same as in Refs. 27 and 28. The present approach for iron has been shown to successfully account for the properties of point defect in iron,[27,29] as well as in Fe containing carbon,[28] phosphorus,[30] or helium.[31] The cutoff radius for the pseudopotential of Al is set to 0.95 Å, 1.00 Å, and 1.15 Å for 3s, 3p, and 3d, respectively. Two localized functions for the 3s states and six for the 3p states have been considered to define the basis set. The cutoff radii are 3.3 Å and 4.3 Å, respectively. In addition, five functions for the 3d states are included as polarized orbitals. As shown in Table I, the physical properties obtained for a fcc Al with our approach are in excellent agreement with other DFT results and experimental data. In the present table, the vacancy formation energy in a pure system X is defined as follows:

$$E_V = E[(N-1)X+1V] - (N-1)E[X], \quad (1)$$

where $E[(N-1)X+1V]$ is the energy of a supercell containing $(N-1)$ atoms of X and one vacancy V in the fcc structure, and $E[X]=E[NX]/N$ is the energy per X atom in the same structure. All the calculations have been done in a bcc supercell containing 128 atom sites. The complete validation of the basis set and the pseudopotential need to be tested as well in the binary system. We have then studied different situa-

TABLE I. Physical properties of Al with the fcc structure. Calculated lattice parameter (a_0), bulk modulus (B), and energy of formation for the vacancy (E_V) are reported.

	a_0 (Å)	B (GPa)	E_V (eV)
Present work	4.04	72	0.54
Other DFT calculation[a]			0.547, 0.55
Experimental[b]	4.04	75	0.67 ± 0.03

[a]References 32 and 33.
[b]Reference 34.

tions which are presented in details in the next section. For the structural defects, some comparisons have been carried out using only 16 and 54 atoms in order to put forward the impact of the interaction between their images due to the periodic boundary conditions. Integrations over the Brillouin zone are based on a $5\times5\times5$, $4\times4\times4$, and $3\times3\times3$ Monkhorst-Pack three-dimensional grid, respectively, for 16, 54, and 128 atom cells. The Methfessel-Paxton scheme is used with a 0.3 eV width. We have verified that this is sufficient to ensure the numerical convergence of all the calculated properties. The calculations have been performed at zero pressure, i.e., the relaxation of the atoms and the shape of the simulation cell are considered using the conjugate gradient minimization scheme. The atomic positions are relaxed until the magnitude of the forces on all the atoms are smaller than 0.04 eV/Å. Last, all the projected density of states (PDOS) presented have been obtained with a peak width of 0.2 eV for broadening the eigenvalues. PDOS plots show both negative and positive scales corresponding to the two different spin components.

III. ENERGETIC, ELECTRONIC, AND MAGNETIC PROPERTIES OF Fe-Al ALLOYS

A. From the infinite dilution to the B2 structure

In order to check the accuracy of our localized-basis-set DFT approach to describe the bonding characteristics in different FeAl alloys, we have chosen to study two limiting cases, i.e., the infinite solution and the widely studied stoichiometric B2 system.

First, we consider the effect of the dissolution of a Al atom in a bcc matrix. In the present work, the solution enthalpy, ΔH_{sol}, is found to be −0.93 eV/atom which is close to the −0.90 eV/atom found by Shalaeva *et al.*[16] using first-principles calculations. ΔH_{sol} is defined as follows:

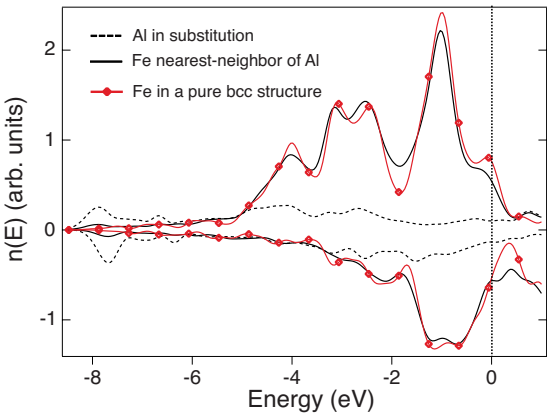

FIG. 1. (Color online) Projected density of states of iron in a perfect bcc structure (full line with circles) and Al in substitution (dotted line) and its nearest neighbor of Fe (full line).

$$\Delta H_{sol} = E_{\mathrm{bcc}}(n\mathrm{Fe} + \mathrm{Al}) - nE_{\mathrm{bcc}}(\mathrm{Fe}) - E_{\mathrm{fcc}}(\mathrm{Al}), \qquad (2)$$

where $E_{\mathrm{bcc}}(n\mathrm{Fe}+\mathrm{Al})$ is the total energy of the mixed Fe+Al system containing nFe atoms and one Al atom in substitution in the bcc structure, $E_{\mathrm{bcc}}(\mathrm{Fe})$ is the energy per atom of the bcc Fe, and $E_{\mathrm{fcc}}(\mathrm{Al})$ is the energy per atom of the fcc Al. From an electronic structure point of view, a narrow band (around −8 eV below the Fermi energy which is set to zero) is formed at low energy due to the presence of the Al atom whereas the PDOS of a neighboring Fe atom remain almost unchanged if compared with pure iron (Fig. 1).

As mentioned previously, to go beyond in the understanding of the Fe-Al interactions, it is very convenient to study the electronic structure properties of an ordered B2 FeAl intermetallic alloy. This structure is a superposition of two simple cubic cells (of Fe and Al) translated by (0.5, 0.5, 0.5) a_0, where a_0 is the lattice parameter. Thus, extensive thermodynamic data and electronic structure calculations are available in the literature. For the B2 structure, our *ab initio* calculations yield an equilibrium lattice parameter at $a=2.91$ Å, an enthalpy of formation $\Delta H_{B2}=-0.32$ eV/atom, and a bulk modulus $B=175$ GPa, where ΔH_{B2} is defined as follows:

TABLE II. Calculated and measured equilibrium lattice parameters (a_0), bulk modulus (B), enthalpies of formation (ΔH_{B2}), and magnetic moments (m_{tot}) for FeAl B2 phase.

	a_0 (Å)	B (GPa)	ΔH_{B2} (eV/atom)	m_{tot} (μ_B)
Present work (GGA)	2.91	175	−0.32	0.75
Other GGA calculations[a]	2.87, 2.83, 2.88	117, 177, 198	−0.33, −0.34	0.72, 0.71
Experimental[b]	2.86, 2.88	152	−0.33	

[a]References 10, 14, 16, and 17.
[b]References 35 and 36.

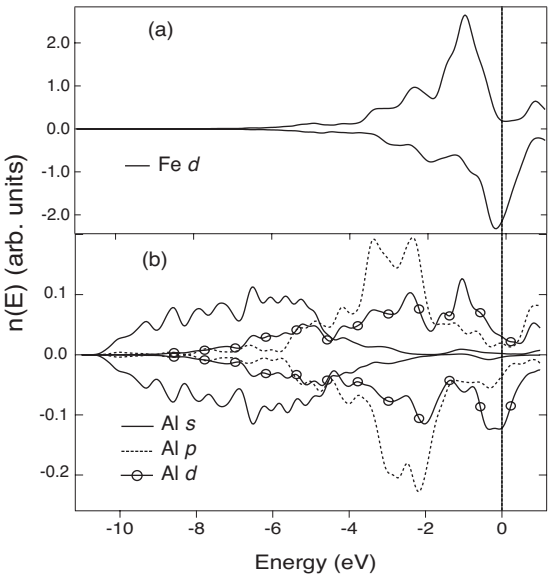

FIG. 2. B2 FeAl. Projected density of states of (a) Fe and (b) Al.

$$\Delta H_{B2} = E_{B2}\left(\frac{n}{2}\mathrm{Fe} + \frac{n}{2}\mathrm{Al}\right) - \frac{n}{2}E_{\mathrm{bcc}}(\mathrm{Fe}) - \frac{n}{2}E_{\mathrm{fcc}}(\mathrm{Al}), \quad (3)$$

$E_{B2}(\frac{n}{2}\mathrm{Fe}+\frac{n}{2}\mathrm{Al})$ is the total energy of the mixed Fe+Al system containing $\frac{n}{2}$ Fe atoms and $\frac{n}{2}$ Al atom in the bcc structure, $E_{\mathrm{bcc}}(\mathrm{Fe})$ is the energy per atom of the bcc Fe structure, and $E_{\mathrm{fcc}}(\mathrm{Al})$ is the energy per atom of the fcc Al structure. Our results agree well with both well-known experimental data and previous *ab initio* results, as shown in Table II. The ground state of the FeAl alloy in a B2 structure is magnetic where the Fe and Al atoms show a local magnetic moment of $0.85\mu_B$ and $-0.10\mu_B$, respectively. The total magnetism obtained is $0.75\mu_B$ per unit cell which is in good agreement with previous DFT calculations (Table II). The PDOS plotted in Figs. 2(b) and 2(c) give more information. At high energy (−2 eV below the Fermi energy) appears the hybridized *pd* band leading to strong bonds in the FeAl structure. At lower energy (typically −8 eV below the Fermi level), there is a slight hybridization between the *s* states of aluminum and the tail of the *d* states of iron.

In the literature, some properties of elementary defects have been reported previously.[37,38] It is well established from these studies that their presence has significant influence on the material properties.[1,4,39] It is then interesting to test the validation of our localized-basis-set DFT on their properties. The most frequent defects occurring in the B2 phase are studied with a primary focus on their formation energies, as well as their electronic and magnetic properties. Two types of defects have been considered in the present work: vacancies and antisite (AS) defects. The formation energy of a *A* vacancy, E_V^A, in a B2 structure is defined as follows:

$$E_V^A = E_{B2}\left[\left(\frac{n}{2}-1\right)A + \frac{n}{2}B\right] - \left(\frac{n}{2}-1\right)E(A) - \frac{n}{2}E(B), \quad (4)$$

where $E_{B2}[(\frac{n}{2}-1)A+\frac{n}{2}B]$ is the total energy of the mixed Fe+Al system in the B2 structure containing $(\frac{n}{2}-1)A$ and $\frac{n}{2}B$, $E(A)$ and $E(B)$ are the energies per atom of the bcc structure for Fe and fcc structure for Al. The formation energy of an antisite defect of *A*, E_{AS}^A, is given by

$$E_{\mathrm{AS}}^A = E_{B2}\left[\left(\frac{n}{2}-1\right)A + \left(\frac{n}{2}+1\right)B\right] - \left(\frac{n}{2}-1\right)E(A) - \left(\frac{n}{2}+1\right)E(B), \quad (5)$$

where $E_{B2}[(\frac{n}{2}-1)A+(\frac{n}{2}+1)B]$ is the total energy of the mixed Fe+Al system in the B2 structure containing $(\frac{n}{2}-1)A$ and $(\frac{n}{2}+1)B$. Although several theoretical works have been devoted to the study of these defects in FeAl, controversial theoretical data are present in the literature. As seen in Table III, large discrepancies have been noticed. This is particu-

TABLE III. Comparison of the calculated results for the energy of formation of vacancies and antisite defects in B2 FeAl. Exchange-correlation functionals, the treatment of relaxation, and magnetism as well as the supercell sizes (in parentheses) are reported. E_V^{Fe}, E_V^{Al}, $E_{\mathrm{AS}}^{\mathrm{Fe}}$, and $E_{\mathrm{AS}}^{\mathrm{Al}}$ are the formation energies of a Fe vacancy, Al vacancy, antisite defect of Fe, and antisite defect of Al, respectively. Values are in electron volt.

		E_V^{Fe}	E_V^{Al}	$E_{\mathrm{AS}}^{\mathrm{Fe}}$	$E_{\mathrm{AS}}^{\mathrm{Al}}$
GGA	Spin-polarized const. vol. (Ref. 16)	0.90 (16)	3.25 (16)	0.70 (16)	0.64 (16)
	Spin-polarized const. press. (Refs. 18 and 40)	0.36 (128)	1.62 (128)	0.60 (128)	0.61 (128)
		0.86 (54)	2.41 (54)	0.61(54)	0.82 (54)
	Nonmagnetic const. vol. (Refs. 21 and 22)			1.054 (16)	0.699 (16)
		1.45 (16)	4.69 (16)	0.748 (16)	1.156 (16)
	Nonmagnetic const. press. (Ref. 18)	0.78 (128)	3.09 (128)	0.80 (128)	0.81 (128)
LDA	Spin-polarized const. vol. (Ref. 23)	0.60 (137)	4.32 (137)		
	Spin-polarized const. press. (Ref. 18)	0.70 (128)	2.78 (128)	0.64 (128)	0.64 (128)
	Nonmagnetic const. vol. (Refs. 19 and 20)	0.97 (32)	4.00 (32)	1.03 (32)	0.95 (32)
		1.06 (54)	3.46 (54)	0.99 (54)	0.99 (54)
	Nonmagnetic const. press. (Ref. 18)	0.96 (128)	3.51 (128)	0.92 (128)	0.92 (128)

TABLE IV. Energy of formation of vacancies, antisite defects in B2 FeAl calculated for 16, 54, and 128 atoms.

	E_V^{Fe}	E_V^{Al}	E_{AS}^{Fe}	E_{AS}^{Al}
16 atoms	0.77	2.86	0.70	0.69
54 atoms	0.73	1.97	0.68	0.67
128 atoms	0.72	2.00	0.66	0.65

larly important for the formation energy of an Al vacancy ranging from 1.62 to 4 eV. In order to clarify this point, we have undertaken a detailed study of defects in the FeAl B2 structure. The goal is to obtain a precise description by avoiding possible artifacts linked to the limitations of previous DFT calculations, i.e., considering complete relaxation of the system, magnetic effects, and sufficient large supercells. Our results, listed in Table IV for different supercells, demonstrated that a system containing 54 atoms was necessary to obtain converged results. In particular, our calculations predict a lower formation energy for the Al vacancy as compared with *ab initio* data found in the literature. For this defect, we have calculated a formation energy equal to 2.86 eV and 2.00 eV for 16 and 128 atom sites, respectively. However, values ranging from 2.78 to 4.69 eV for the latter one are reported, excepted the 1.62 eV found by Besson *et al.*[18] This may not be surprising; many factors, such as magnetism, size of the system, or relaxation effect can play a role. Indeed, as illustrated in Table IV, the size of the supercell can have a strong influence. Yet, the first calculations were performed on small systems containing 16 atoms, where relaxations were neglected. This last point can have a crucial importance. In order to point out this specific feature, the local relaxations around the defects are investigated. The relative displacements are presented in Fig. 3 for different defects and supercells. On one hand, we have found that the local relaxation of the first neighbors Al atoms around the Fe vacancy is an inward shift [Fig. 3(a)]. This value is only about 3% of the equilibrium lattice parameter of the extended FeAl B2 phase with the vacancy and vary slightly with the size of the system. We have quantitatively observed the same tendency for the antisite defects with even weaker deformation around the defect and small dependence with the simulation cell size [Figs. 3(c) and 3(d)]. On the other hand, a vacancy of Al induces local strain leading to strong distortions of the surrounding lattice, contrary to the other defects. In Fig. 3(b), the deformation observed is around 10% for 54 and 128 atoms. This strain field, caused by the vacancy, has an important effect on first neighbors, as well as on second neighbors of the vacancy on the Al site. Thus, a small supercell with 16 atoms is not enough to compensate this effect. For this reason, the local relaxations devoted to the study of defects present in the FeAl B2 phase cannot be neglected. Another interesting feature to consider here concerns the effect of the magnetism. In the ordered B2-type structure, many theoretical studies have discussed the magnetism in bcc-based $Fe_{1-x}Al_x$.[6,11,18,41,42] To go further, we have analyzed the modified local magnetism of iron atoms close to the defect induced by the vacancies and the antisite defects. The results can be shown through the PDOS as presented in Fig. 4. For the vacancy of Fe, only the local magnetic moment of the first Al neighbors are slightly affected [Fig. 4(a)]. From the second neighbors, the electronic density of states and the local magnetic moment of the atoms remain practically unchanged compared with the perfect B2 structure. The situation is rather different in the case of the Al vacancy where the local magnetic moment of the first and the second neighbors of the defect are modified, as shown in Fig. 4(b). This is in good agreement with the previous analysis where important lattice distortions have been observed. Yet, it is well known that the local magnetic moment and the corresponding atomic volume as well as the chemical environment are directly correlated. Indeed, the local magnetic moment tends to increase with increasing coordination or increasing interatomic distance. Finally, Figs. 4(c) and 4(d) show PDOS which allow to review the local magnetic moment changes close to the antisite. More precisely, the antisite Fe atom has a very high local magnetism [Fig. 4(d)]. This is mainly due to the local environment of this defect which is the same as in pure bcc iron. This defect has a magnetic moment equal to $2.26\mu_B$ which is close the value of $2.30\mu_B$ observed in pure bcc iron.

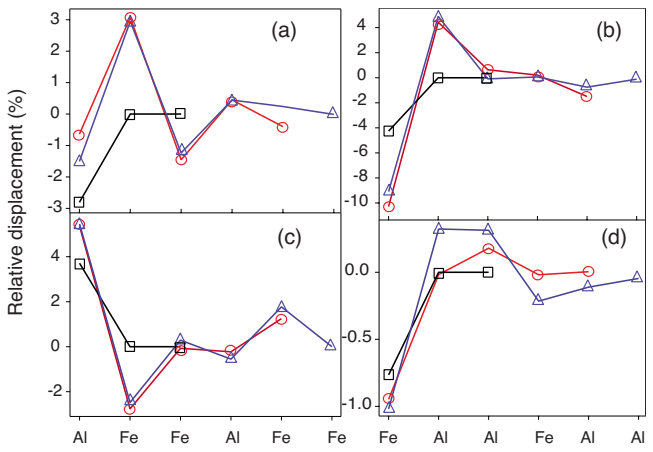

FIG. 3. (Color online) Relative displacements of the atoms surrounding the defect as function of the nature of the atoms as they localized around the defect. (a) Fe vacancy, (b) Al vacancy, (c) AS Al, and (d) AS Fe. The squares, circles and triangles are for supercells containing 16, 54, and 128 atoms, respectively.

B. Relative phase stability at 0 K

To understand how order affects the energetics of this alloy we have compared ordered structures to random structures as obtained following the special quasirandom structures methodology (SQS).[43] We have considered a supercell containing 128 atoms for a concentration of Al varying from 0% to 50%. Due to the fact that the number of configurations to be explored increases significantly with the number of atoms, the representative random structures employed in these calculations were obtained by generating around 10^4 configurations for each concentrations. We have calculated the set of short-range correlation, namely, the pair correlations up to the eighth neighbors, the correlations for triplets to the third neighbors and quadruplets up to first nearest

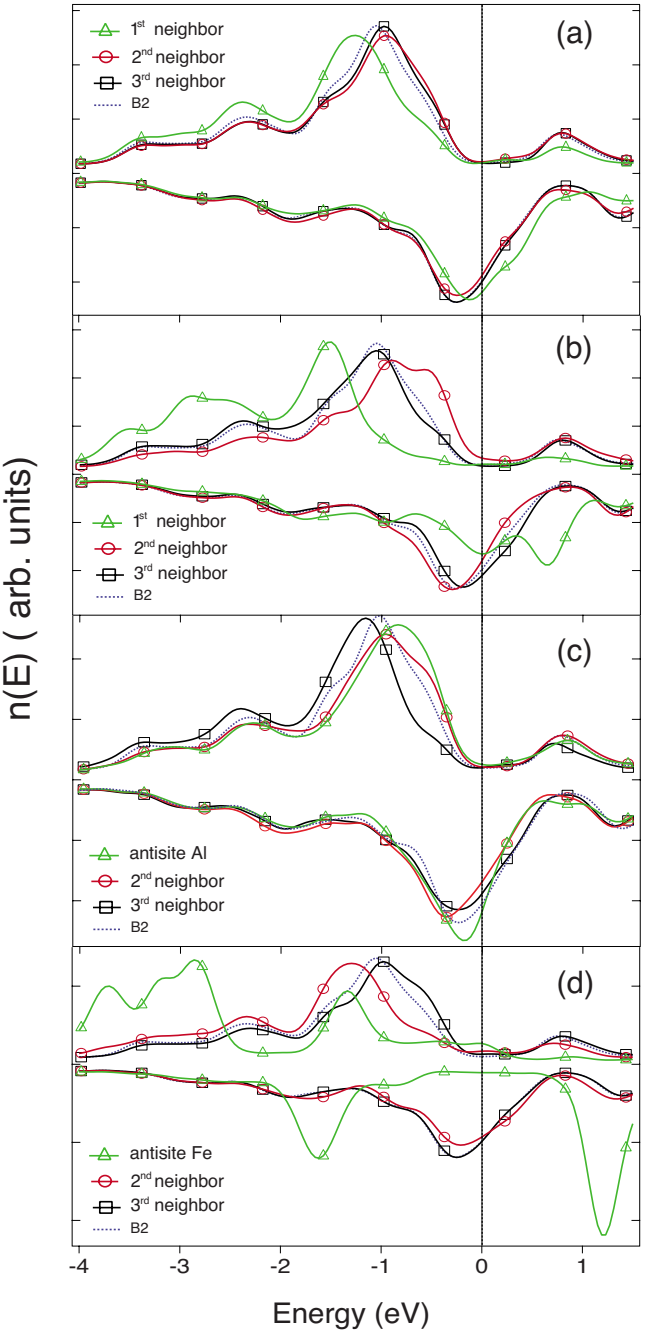

FIG. 4. (Color online) PDOS calculated for different Fe atoms present around the defect compared with Fe atom in the perfect B2 structure. The defects are (a) Fe vacancy, (b) Al vacancy, (c) antisite Al, and (d) antisite Fe.

neighbors, for each structure. These correlation functions have been compared with those as given for a infinite random system. The set of correlation functions were calculated using the ATAT package.[44] Choosing as representative random structure the one with the lowest difference in short-range order. In this way, we obtain a good representation of solid solutions with various concentrations. We have then calculated the mixing enthalpy of the system. The results are plotted in Fig. 5. The enthalpy of mixing, ΔH_{mix}, is defined as follows:

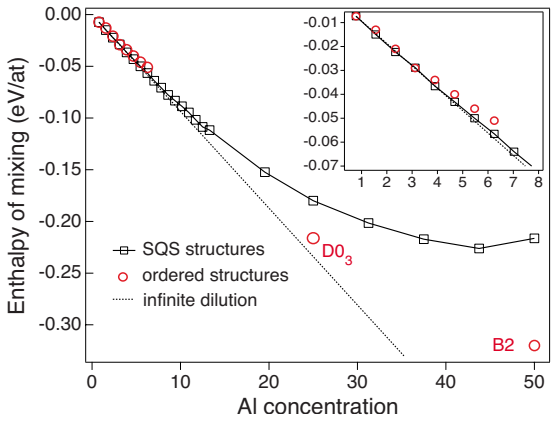

FIG. 5. (Color online) Enthalpy of mixing at 0 K.

$$\Delta H_{mix} = \frac{E_{\mathrm{bcc}}(n\mathrm{Fe} + m\mathrm{Al}) - [nE_{\mathrm{bcc}}(\mathrm{Fe}) + mE_{\mathrm{fcc}}(\mathrm{Al})]}{n+m}, \quad (6)$$

where $E_{\mathrm{bcc}}(n\mathrm{Fe}+m\mathrm{Al})$ is the total energy of the mixed Fe+Al system containing nFe atoms and mAl atoms in substitution in the bcc structure, $E_{\mathrm{bcc}}(\mathrm{Fe})$ is the energy per atom of the bcc Fe and $E_{\mathrm{fcc}}(\mathrm{Al})$ is the energy per atom of the fcc Al. A positive value of ΔH_{mix} corresponds to a phase separation tendency and a negative one to an ordering tendency. In the present case, as the aluminum concentration in iron increases, the absolute value of the enthalpy of mixing decreases substantially and remains negative over the entire concentration range, meaning that the Fe-Al bonds are favored with respect to Fe-Fe and Al-Al bonds. We can see in the same figure two different regimes. First, for small concentrations (below 10%) SQS structures are favored. Thus, dilute systems appear at the expense of ordered structures. Then the situation is changing with the stabilization of ordered structures up to the formation of the B2 structure for a concentration of Al equal to 50%. In between, the most stable configuration which is below the infinite dilution limit is given at a Al concentration of 25% which corresponds to the D0$_3$ phase. Therefore, attraction between Al atoms exists at 0 K stabilizing ordered structures such as B2 and D0$_3$ phases with sufficient large Al concentration although Al-Al first and second neighbors are repulsive in the dilute case (see Sec. IV). All those 0 K results are indeed compatible with the generally accepted phase diagram,[45] where the B2 and D0$_3$ phases are ordered structures within the bcc lattice. To go beyond, a more complete set of calculations including the temperature effects are required as discussed in Refs. 12 and 46.

IV. ALUMINUM-VACANCY CLUSTERS

A. Al-Al and Al-V interactions in iron

As a first step to understand the behavior of $V_n\mathrm{Al}_m$ complexes, the interactions between Al atoms and the vacancies in α-iron must be understood. In order to quantify them, we have calculated the binding energies $E_{XY}^{b(n)}$ between X and Y, lying on nth nearest-neighbor sites. $E_{XY}^{b(n)}$ is defined as follows:

TABLE V. Binding energies for Al-Al and Al-V pairs. First-, second-, and third-nearest-neighbor interactions are considered. Values are given in electron volt.

	First neighbor	Second neighbor	Third neighbor
Al-Al	−0.117	−0.123	+0.007
Al-V	+0.288	+0.033	+0.008

$$E_{XY}^{b(n)} = E[(N-1)A+1X] + E[(N-1)A+1Y] - E[NA] - E[(N-2)A+1X+1Y], \quad (7)$$

where $E[(N-2)A+1X+1Y]$ is the total energy of a supercell containing N sites, $(N-2)$ A atoms, and one X-Y pair. Note that the positive value means attraction. The results for Al-Al and Al-V pairs are presented in Table V. We have found that the interaction between Al atoms is repulsive for all interatomic distances: −0.117 eV and −0.123 eV, for the first and second neighbors, respectively. From the third neighbor, the interaction practically vanishes with a binding energy close to zero. The situation is different in presence of vacancy. Al atom and vacancy attract each other forming stable binary complexes. The interaction between them is strong only at short distance with a binding energy equal to +0.288 eV and then vanishes between second-nearest neighbor Al-V pair (+0.032 eV). In order to understand, those results, PDOS of different electronic states have been analyzed for Fe-Al bonds in distinct environments. Since the presence of an Al atom in substitution leads to a negligible distortion of the crystal, this investigation becomes relevant. The first case studied is the infinite dilution of Al in iron. As shown in Fig. 6(a), we see clearly that at low energy there is a narrow band derived from the 3s states of aluminum. Then, at higher energy appears the p band which, as mentioned previously forms a pd band with the iron. Moreover, it is interesting to notice that hybridization $2s_{\mathrm{Al}}$-$2p_{\mathrm{Al}}$ bonding between 2s and 2p states of Al is still present in this case. We have observed that the Al atom shows a magnetic moment of $-0.21\mu_B$, whereas the Fe atoms close to it have a magnetic moment of $2.30\mu_B$. For the Al-V pair, the $2s_{\mathrm{Al}}$-$2p_{\mathrm{Al}}$ bond is indeed stronger, as shown in Fig. 6(b). The width of the s band located at low energy is larger leading to a stronger interaction with the p band. In the present case, the Al atom has a magnetic moment equal to $-0.26\mu_B$. For the first neighbors of Fe, this quantity varies from $2.19\mu_B$ to $2.38\mu_B$ depending on their position in relation to the vacancy. For the Al-Al first-neighbor pair, plotted in Fig. 6(c), the conclusions are different. There is still a narrow band at low energy. However, this band is shifted to lower energy. This shift, due to the interaction between Al atoms, leads to the decreasing of the $2s_{\mathrm{Al}}$-$2p_{\mathrm{Al}}$ hybridization. We have observed a magnetic moment of $-0.21\mu_B$ for the Al atoms, whereas the Fe atoms close to the pair have a magnetic moment ranging from $2.28\mu_B$ to $2.30\mu_B$. This local analysis suggests that the $2s_{\mathrm{Al}}$-$2p_{\mathrm{Al}}$ bond is the key parameter which explains the stability of the Al-V pairs and the instability of Al-Al pairs in iron. To quantify this effect, bond orders between an Al atom and its nearest neighbors of iron have been analyzed (see Table VI). The bond orders are estimated by considering the off-diagonal elements of the Mulliken atomic overlaps population matrix resulting from SIESTA calculations, which correspond to the charge accumulation between different atoms. This is a good indication of bond strength between atoms as discussed in detail by Pettifor.[47] The differences of values shown in Table VI are significant providing that the error bars due to numerical precision are estimated to be around 0.01 eV. We note that the bond order is stronger between an Al atom and its first neighbor for the Al-V pair. This is still true for the second neighbor where the bond order is significant, contrary to other cases, explaining the broadening of the 3s band for the Al atom observed in Fig. 6(b). The stability of Al-V complexes is mainly driven by a significant interaction between the Al atom and its first and second neighbors.

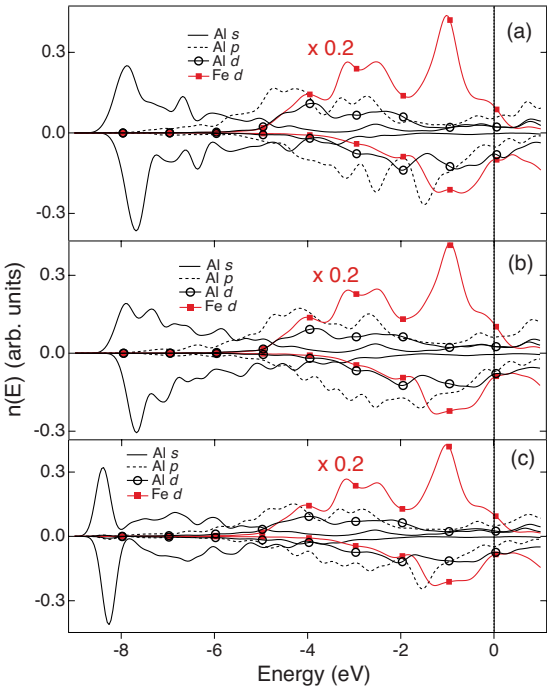

FIG. 6. (Color online) PDOS calculated for (a) Al in Fe, (b) Al-V in Fe, and (c) Al-Al in Fe. The values corresponding to orbitals d of Fe are multiplied by 0.2.

B. Stability of small $V_n\mathrm{Al}_m$ clusters

According to the previous part, we have seen in a dilute FeAl system that the interaction between close Al pairs is always repulsive. This means that an Al atom does not like to be close to another Al atom. Furthermore, the presence of

TABLE VI. Bond order between an Al atom and its nearest neighbors of iron following the Mulliken criterion.

Al-Fe	Al in substitution	Al-Al	Al-V
First neighbor	0.14	0.13	0.14–0.15
Second neighbor	0.06	0.06–0.07	0.11–0.12

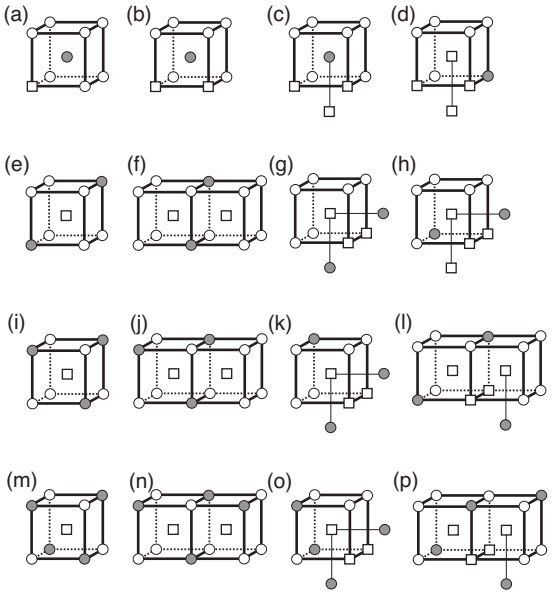

FIG. 7. Schematic representation of the lowest-energy configurations found from DFT calculations for: (a) VAl, (b) V_2Al, (c) V_3Al, (d) V_4Al, (e) VAl$_2$, (f) V_2Al$_2$, (g) V_3Al$_2$, (h) V_4Al$_2$, (i) VAl$_3$, (j) V_2Al$_3$, (k) V_3Al$_3$, (l) V_4Al$_3$, (m) VAl$_4$, (n) V_2Al$_4$, (o) V_3Al$_4$, and (p) V_4Al$_4$. The gray spheres denote Al atoms, empty spheres are the neighboring Fe atoms, and the empty cubes symbolize the vacancies.

vacancy attracts Al atoms with a high binding energy. Then, vacancy has a strong tendency to occupy sites close to Al atoms. According to these arguments, the building of V_nAl$_m$ clusters is simplified. All we have to do is to start from known V_n clusters[48] and to construct large clusters step by step by considering those simple rules. The methodology followed here for the generation of structures is very useful to avoid the need for checking a large number of different configurations. V_nAl$_m$ complexes with n, and $m=1$, 2, 3, or 4 were considered in this study. In order to determine their lowest-energy configurations (Fig. 7), we have investigated up to five structures for each binary complex, based on the previous conclusions. Schematic representation of the lowest-energy configurations for small complexes are presented in Fig. 7. Some characteristics of the lowest-energy structures found for V_nAl$_m$ clusters are interesting to be pointed out. We can observe that for one vacancy, the most stable structure is the positioning of Al atoms around it without direct interaction between Al atoms. See Figs. 7(a), 7(e), 7(i), and 7(m), where AlV, Al$_2V$, Al$_3V$, and Al$_4V$ are represented. This is still true when the number of V is increasing. Al atoms stay at substitutional positions decorating the vacancies, as shown in Fig. 7 V_2, V_3, and V_4. To go beyond, binding energies corresponding to V_nAl$_{m-1}$+Al$\rightarrow V_n$Al$_m$ and V_{n-1}Al$_m+V\rightarrow V_n$Al$_m$ are detailed in Fig. 8, where positive values mean attractions. The vacancy and Al binding energies to the cluster are found to be positive in all cases, i.e., all interactions are attractive. For one vacancy, the Al binding energy is roughly independent of the number of Al atoms in the cluster and close to the binding energy of an Al atom to a vacancy, 0.288 eV, calculated previously [see Fig. 8(a)]. From $n=2$, the Al binding energies are stronger simply because the Al atom can form two direct bonds with vacancies which are strong. However, the energy gain associated to the inclusion of one Al atom into a more complex cluster is configuration dependent. Thus, the incorporation of a second Al atom is larger for $n=2$, 3, and 4 for the same reason explained before. Moreover, in this configuration, the system can form strong Al-V bond without creating direct interaction between Al atoms. From $m=3$, the Al binding energy decreases, due to the interaction between Al-Al atoms at short range. Conclusions are slightly different for the binding of vacancies to V_nAl$_m$ complexes as plotted in see Fig. 8(b). For $n=1$, the V binding energy increases as a function of the number of Al atoms. However for larger n, the energy gain is independent of the amount of Al atoms presents in the cluster. Thus, we can observe that V-to-complex binding energies are often higher than Al-to-complex interaction, which is consistent with the fact that Al-Al interaction are repulsive at short range. All this analysis implies that the presence of Al helps the nucleation of V clusters.

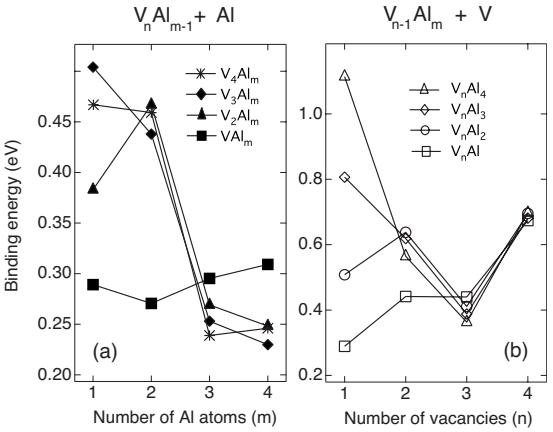

FIG. 8. Binding energies of an Al atom and a vacancy to (a) V_nAl$_{m-1}$ and (b) V_{n-1}Al$_m$ complexes, respectively. Positive values indicate attractive interactions.

The high stability of V_nAl$_m$ suggests that Al may significantly modify the vacancy concentration, especially after a quench from a high temperature T_0 to $T\ll T_0$. Actually, the evolution of the total vacancy concentration $[V_T]$ depends on the speed of the quench and on the efficiently and density of the vacancy sinks (dislocations, grain boundaries, etc.) available in the alloy microstructure. A complete treatment of the problem is beyond the scope of this study but preliminary conclusions can be drawn by comparing two limiting cases. First, the quench is sufficiently slow and the sinks density is sufficiently high so that the evolution of vacancy concentration is rapid and reach the equilibrium value at T. In the second case, the quench is very rapid and the sinks density is very low (well below the concentration of small Al clusters): the vacancies cannot annihilate so that the total vacancy concentration remains at its initial equilibrium value at T_0 but the vacancies can redistribute between the clusters. In both situations, clusters concentrations are given by the mass-action law,

$$[V_n\mathrm{Al}_m]=[V]^n[\mathrm{Al}]^m\exp(E_b/k_BT), \tag{8}$$

E_b is the total binding energy to form V_nAl$_m$ from n vacancies and m isolated aluminum atoms defined in Eq. (7) and

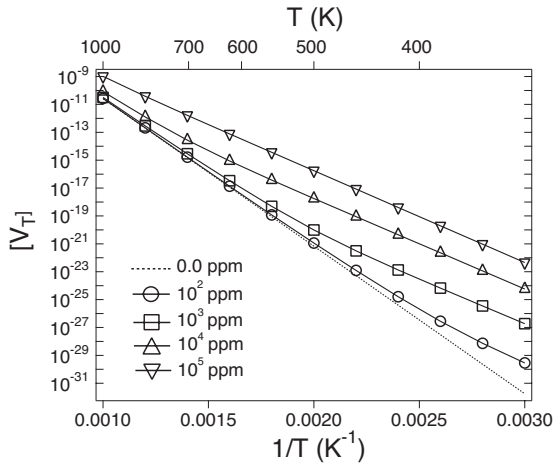

FIG. 9. Variation in the total vacancy concentrations $[V_T]$ as a function of temperature from 0.0 to 10^5 ppm Al.

k_B is the Boltzmann constant. The total concentration of aluminum $[\mathrm{Al}_T]=\Sigma_{n,m} m[V_n\mathrm{Al}_m]$ being constant.

In the first case the concentration of isolated vacancies at T is imposed by their formation energy given by $[V_1]=\exp(-E_f^V/k_BT)$, where $E_f^V=2.12$ eV according to our DFT calculations. The resulting $[V_T]$ are shown in Fig. 9, for Al concentration ranging from 10^2 to 10^5 ppm. We note that, besides the Al free cases, the curves exhibit deviation from an Arrhenius behavior when the Al content is small. Also, the total vacancy concentration increase with Al content, which means a decrease in the corresponding effective vacancy formation energy assuming an Arrhenius law at given ranges of temperatures.

For a very rapid quench, corresponding to the second case, the total vacancy concentration is imposed by the initial value $[V_1]=\exp(-E_f^V/k_BT_0)$. This situation is close to experimental conditions where vacancies are formed upon rapid quenching from elevated temperatures. Examples of the final concentration of clusters $[V_n\mathrm{Al}_m]$, for a quench from $T_0=1000$ K to T and in alloys with 10 and 10^5 ppm of Al are given in Fig. 10. There is always an excess of Al atoms with respect to vacancy by many orders of magnitudes. As shown in Fig. 10, most complexes are dissociated at high temperatures and isolated vacancies are indeed the dominant species. At this temperature, we also observe a significant presence of $V\mathrm{Al}_m$ clusters for high concentration of Al whereas their quantity is lower for 10 ppm of Al. Indeed, in the former case, we have many Al atoms in the system leading to Al_2 or Al_3 complexes and also the formation of these $V\mathrm{Al}_m$ clusters which are very stable. On the opposite side, at low temperatures, all the vacancies are trapped in immobile complexes. The dominant species as function of temperature depend essentially on the specific Al content and on the free binding energies which have two contributions: an energetic and an entropic contribution. In this simple model, we have only included the configurational entropy while the vibrational binding entropic part have been neglected. A treatment of the problem where those effects are included is beyond the scope of this study and will not modify the discussion presented in this work. This will probably change the temperature of transition between different regimes and the specific dominant

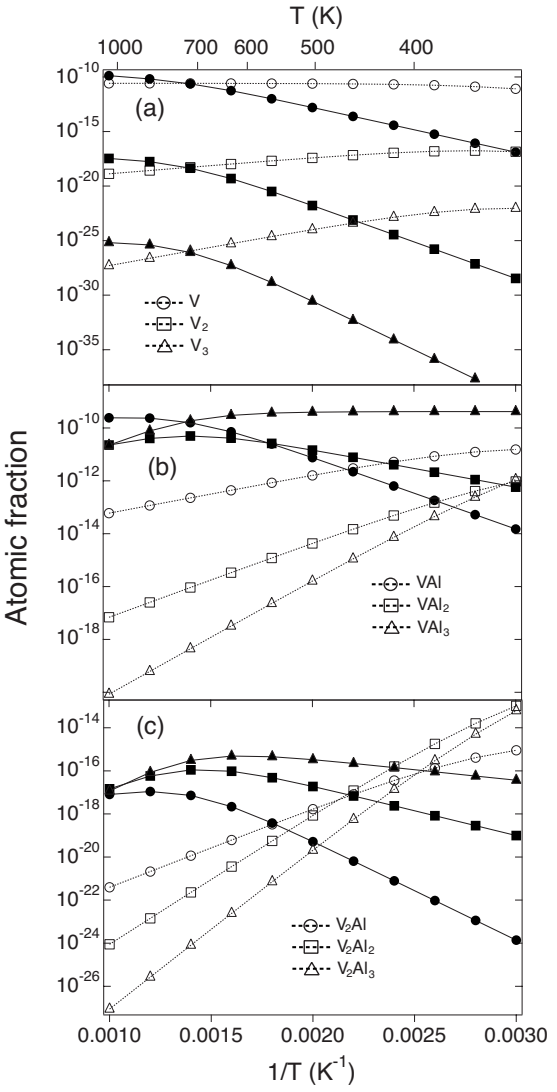

FIG. 10. Variation in different $V_n\mathrm{Al}_m$ complexes atomic fractions as a function of the quenching temperature from 1000 K for iron containing 10 ppm (dotted line) and 10^5 ppm (full line) Al: (a) V_n, (b) $V\mathrm{Al}_m$, and (c) $V_2\mathrm{Al}_m$.

clusters at intermediate temperatures but the overall trends in Figs. 9 and 10 will be the same. In particular, we observe a regime where $V_n\mathrm{Al}_m$ species are stabilized. According to this simple thermodynamic model, the present results reveal the presence of various $V_n\mathrm{Al}_m$ clusters in very dilute systems.

V. MOBILITY OF ALUMINUM IN IRON

To go beyond the thermodynamic properties of Fe-Al alloys, we have investigated the diffusion properties of Al solutes in iron. Thus, the interaction energies and the migration barriers obtained by using DFT calculations are integrated in the theory of diffusion in dilute alloy using the Le Claire's diffusion model.[49,50] This approach is described in detail elsewhere.[51,52]

According to Le Claire's diffusion model, the self-diffusion coefficient and the diffusion coefficient of an Al impurity in an α-iron crystal can be expressed through ana-

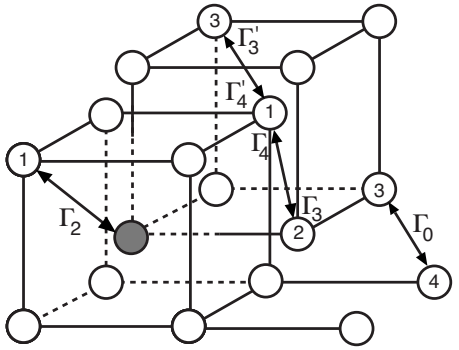

FIG. 11. Vacancy jump frequencies (Γ_i) around an aluminum atom (gray) and its neighboring iron atoms (white). The arrows indicate the direction of the vacancy jumps; the circled numbers are the order of neighbors to the aluminum atom.

lytical expressions depending on the lattice parameter, the equilibrium in pure iron and the atomic jump frequencies, Γ_i, of the vacancies. The jump frequency of an atom (A=Fe or Al) on a vacancy (V) located on nearest-neighbor site is given by

$$\Gamma_i = \nu_A \exp\left(\frac{\Delta E_i}{k_B T}\right), \tag{9}$$

where ν_A is an attempt frequency and ΔE_i the migration barrier. The vacancy migration barriers are calculated using the drag method. In this approach, the atomic positions relative to the center of mass have the possibility to relax only in the hyperplane perpendicular to the vector joining the initial and the final positions.[29] When second-nearest-neighbor interactions are neglected, which is the case here, only some jump frequencies must be considered: Γ_0 (Fe-V exchange in pure iron), Γ_2 (Al-V exchange in pure iron), etc. (the definitions and notations are plotted in Fig. 11). The values are presented in Table VII. The self-diffusion coefficient in an α-Fe crystal is given by

$$D_{\mathrm{Fe}} = a^2 \Gamma_0 f_0 C_v^{eq}(\mathrm{Fe}), \tag{10}$$

where a=2.87 Å is the iron lattice parameter, C_v^{eq} the vacancy concentration in the Fe matrix and f_0 the autodiffusion correlation factor (f_0=0.727 in the bcc structure). The diffusion coefficient of an Al impurity in pure α-Fe is given by

TABLE VII. Migration barriers involved in the impurity diffusion coefficient of Al in iron and obtained by means of *ab initio* calculations. Values are in electron volt.

Jump	*Ab initio*
ΔE_0	0.68
ΔE_2	0.47
ΔE_3	0.82
ΔE_4	0.58
$\Delta E'_3$	0.75
$\Delta E'_4$	0.50

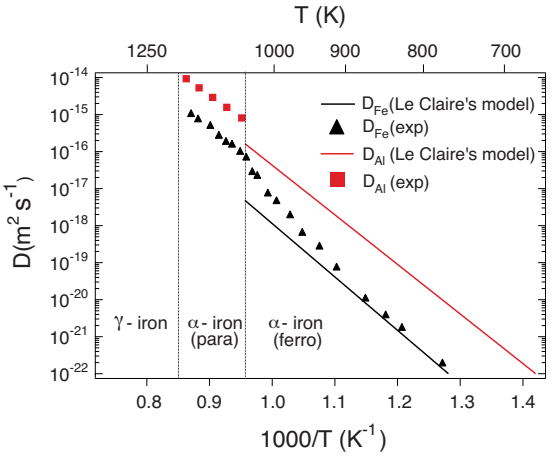

FIG. 12. (Color online) Iron self-diffusion and aluminum impurity diffusion coefficients. Comparison between the experimental data for iron (Ref. 53) and aluminum (Refs. 54 and 55) and the Le Claire's model.

$$D_{\mathrm{Al}} = a^2 \Gamma_2 \frac{\Gamma'_4}{\Gamma'_3} f_2 C_v^{eq}(\mathrm{Fe}), \tag{11}$$

where f_2 is the impurity correlation factor.

The attempt frequencies ν_{Fe} and ν_{Al} are fitted to the experimental diffusion data: the self-diffusion coefficient in ferromagnetic iron (D_{Fe}), the stable state at low temperature. A good agreement is obtained at low temperature (Fig. 12) for $\nu_{\mathrm{Fe}} = \nu_{\mathrm{Al}} = 5 \times 10^{15}$ s^{-1}. This effective attempt frequency is larger than the Debye frequency by 2 or 3 orders of magnitude: it has been suggested[51] that it is because it includes entropic contributions. One important contribution is the vacancy formation entropy (recently estimated to $4.08k_B$ by Lucas and Schaublin[56]), other ones may be expected such as magnetic or electronic contribution, and entropy of migration.

Unfortunately, the Al impurity diffusion coefficient in iron (D_{Al}) has been measured only at high temperatures in paramagnetic bcc iron. Keeping the same attempt frequency $\nu_{\mathrm{Fe}} = \nu_{\mathrm{Al}} = 5 \times 10^{15}$ s^{-1} than for iron gives an Al diffusion coefficient more than ten times larger than the one of Fe (Fig. 12) which seems reasonable, by comparison with the values of D_{Fe} and D_{Al}.

VI. CONCLUSION

The electronic structure and bonding characteristics which come into play in a B2 FeAl alloy and the properties of their elementary structural defects have been investigated. Our study emphasizes that the role of magnetism and relaxation effects in DFT calculations are important to correctly predict the formation energies of defects in this structure. Then, the main part of our work focused on very dilute Fe-Al alloys. According to our *ab initio* calculations and a simple thermodynamic model we have developed, the existence of various $V_n Al_m$ clusters in very dilute systems has been demonstrated. The presence of such clusters is suspected to have a strong influence on the mechanical properties of the material. In-

deed, V_nAl_m complexes can trap edge (or screw) dislocations and then affecting the behavior of dislocations. However, carbon atoms are always present in Fe-based materials, either as impurities even in high-purity samples or as an intrinsic constituent of steels. The presence of carbon atoms may have similar outcomes, i.e., formation of vacancy-carbon attractions. In the next step, it is then necessary to consider a more complex problem by studying the influence of carbon atoms on the thermodynamic stability and the diffusion of $V_nAl_mC_p$ clusters. The approach proposed here can be very useful to gain insights on the atomic scale origin of their mechanical properties degradation.

ACKNOWLEDGMENTS

The authors thank Enrique Martinez for the development of SQS structures. This work was partly performed using HPC resources from GENCI-CINES (Grant No. 2009-x2009096020). P.M. and H.A. thank ArcelorMittal and CIRIMAT/CNRS/INPT for financial support.

[1] J. L. Jordan and S. C. Deevi, Intermetallics **11**, 507 (2003).
[2] D. G. Morris and S. C. Deevi, Mater. Sci. Eng., A **329**, 573 (2002).
[3] C. T. Liu, Mater. Chem. Phys. **42**, 77 (1995).
[4] Y. A. Chang, L. M. Pike, C. T. Liu, A. R. Bilbrey, and D. S. Stone, Intermetallics **1**, 107 (1993).
[5] F. Moret, R. Baccino, P. Martel, and L. Guetaz, J. Phys. IV **6**, 281 (1996).
[6] J. Bogner, W. Steiner, M. Reissner, P. Mohn, P. Blaha, K. Schwarz, R. Krachler, H. Ipser, and B. Sepiol, Phys. Rev. B **58**, 14922 (1998).
[7] D. G. Morris and M. A. Morris-Muñoz, Intermetallics **7**, 1121 (1999).
[8] J. Kansy, A. Hanc, D. Giebel, and M. Jabłońska, Acta Phys. Pol. A **113**, 1409 (2008).
[9] M. Hillert and M. Selleby, J. Alloys Compd. **329**, 208 (2001).
[10] D. Fuks, A. Strutz, and A. Kiv, Intermetallics **14**, 1245 (2006).
[11] A. V. Smirnov, W. A. Shelton, and D. D. Johnson, Phys. Rev. B **71**, 064408 (2005).
[12] B. Sundman, I. Ohnuma, N. Dupin, U. R. Kattner, and S. G. Fries, Acta Mater. **57**, 2896 (2009).
[13] D. Fuks, A. Strutz, and A. Kiv, Int. J. Quantum Chem. **102**, 606 (2005).
[14] P. Maugis, J. Lacaze, R. Besson, and J. Morillo, Metall. Mater. Trans. A **37**, 3397 (2006).
[15] D. Connétable and P. Maugis, Intermetallics **16**, 345 (2008).
[16] E. V. Shalaeva, N. I. Medvedeva, and I. R. Shein, Phys. Solid State **49**, 1253 (2007).
[17] C. D. Latham, S. Öberg, P. R. Briddon, and F. Louchet, J. Phys.: Condens. Matter **18**, 8859 (2006).
[18] R. Besson, A. Legris, and J. Morillo, Phys. Rev. B **74**, 094103 (2006).
[19] C. L. Fu, Y.-Y. Ye, M. H. Yoo, and K. M. Ho, Phys. Rev. B **48**, 6712 (1993).
[20] M. Fähnle, J. Mayer, and B. Meyer, Intermetallics **7**, 315 (1999).
[21] A. Strutz, D. Fuks, and A. Kiv, J. Phase Equilib. Diffus. **26**, 529 (2005).
[22] A. Kellou, H. I. Feraoun, T. Grosdidier, C. Coddet, and H. Aourag, Acta Mater. **52**, 3263 (2004).
[23] J.-A. Yan, C.-Y. Wang, and S.-Y. Wang, Phys. Rev. B **72**, 134108 (2005).
[24] A. Broska, J. Wolff, M. Franz, and T. Hehenkamp, Intermetallics **7**, 259 (1999).
[25] R. Kerl, J. Wolff, and T. Hehenkamp, Intermetallics **7**, 301 (1999).
[26] J. M. Soler, E. Artacho, J. D. Gale, A. Garcia, J. Junquera, P. Ordejon, and D. Sanchez-Portal, J. Phys.: Condens. Matter **14**, 2745 (2002).
[27] C.-C. Fu and F. Willaime, Phys. Rev. B **72**, 064117 (2005).
[28] C. C. Fu, E. Meslin, A. Barbu, F. Willaime, and V. Oison, Solid State Phenom. **139**, 157 (2008).
[29] C.-C. Fu, F. Willaime, and P. Ordejon, Phys. Rev. Lett. **92**, 175503 (2004).
[30] E. Meslin, C. C. Fu, A. Barbu, F. Gao, and F. Willaime, Phys. Rev. B **75**, 094303 (2007).
[31] C. J. Ortiz, M. J. Caturla, C. C. Fu, and F. Willaime, Phys. Rev. B **80**, 134109 (2009).
[32] A. De Vita and M. J. Gillan, J. Phys.: Condens. Matter **3**, 6225 (1991).
[33] K. M. Carling, G. Wahnström, T. R. Mattsson, N. Sandberg, and G. Grimvall, Phys. Rev. B **67**, 054101 (2003).
[34] P. Erhart, P. Jung, H. Schult, and H. Ullmaier, in *Atomic Defects in Metals*, Landolt-Börnstein, New Series, Group III Vol. 25, edited by H. Ullmeier (Springer-Verlag, Berlin, 1991).
[35] F. R. de Boer, R. Boom, W. C. M. Mattens, A. R. Miedema, and A. K. Niessen, *Cohesion in Metals: Transition Metal Alloy* (North-Holland, Amsterdam, 1988).
[36] P. Villars and L. D. Calvert, *Pearson's Handbook of Crystallographic Data for Intermetallic Phases* (American Society for Metals, Metal Park, OH, 1986).
[37] T. Haraguchi, F. Hori, R. Oshima, and M. Kogachi, Intermetallics **9**, 763 (2001).
[38] J. H. Schneibel and L. M. Pike, Intermetallics **12**, 85 (2004).
[39] P. Nagpal and I. Baker, Metall. Trans. A **21A**, 2281 (1990).
[40] Complementary DFT plane-wave calculations are performed (54 atoms) with the PWSCF package (S. Baroni, A. Dal Corso, S. de Gironcoli, and P. Giannozzi, http://www.pwscf.org) using an ultrasoft pseudopotential and a plane-wave energy cutoff of 30 Ry.
[41] V. L. Moruzzi and P. M. Marcus, Phys. Rev. B **47**, 7878 (1993).
[42] P. G. Gonzales-Ormeño, H. M. Petrilli, and C. G. Schön, Scr. Mater. **54**, 1271 (2006).
[43] S.-H. Wei, L. G. Ferreira, J. E. Bernard, and A. Zunger, Phys. Rev. B **42**, 9622 (1990).
[44] A. van de Walle, Alloy Theoretic Automated Toolkit (ATAT), http://www.its.caltech.edu/avdw/atat
[45] U. R. Kattner and B. P. Burton, in *Phase Diagrams of Binary Iron Alloys*, edited by H. Okamoto (ASM Internationals, Materials Park, OH, 1993).
[46] D. Connétable, J. Lacaze, P. Maugis, and B. Sundman,

CALPHAD: Comput. Coupling Phase Diagrams Thermochem. **32**, 361 (2008).
[47] D. G. Pettifor, *Bonding and Structure in Molecules and Solids* (Oxford University Press, Oxford, 1995).
[48] C.-C. Fu, J. Dalla Torre, F. Willaime, J.-L. Bocquet, and A. Barbu, Nat. Mater. **4**, 68 (2005).
[49] A. D. Le Claire, in *Physical Chemistry: An Advanced Treatise*, edited by H. Eyring (Academic, New York, 1970), Vol. 10, p. 261.
[50] J.-L. Bocquet, G. Brebec, and Y. Limoge, in *Physical Metallurgy*, edited by R. W. Cahn and P. Haasen (North-Holland, Amsterdam, 1996), Chap. 7.
[51] F. Soisson and C.-C. Fu, Phys. Rev. B **76**, 214102 (2007).
[52] Y. Le Bouar and F. Soisson, Phys. Rev. B **65**, 094103 (2002).
[53] G. Salje and M. Feller-Kniepmeier, J. Appl. Phys. **48**, 1833 (1977).
[54] I. A. Akimova, V. M. Mironov, and A. V. Pokoyev, Fiz. Met. Metalloved. **56**, 1225 (1983).
[55] I. A. Akimova, V. M. Mironov, and A. V. Pokoyev, Phys. Met. Metallogr. **56**, 175 (1983).
[56] G. Lucas and R. Schaublin, Nucl. Instrum. Methods Phys. Res. B **267**, 3009 (2009).